The effect of receiver configuration and velocity perturbation on microseismic event location

Soo-Kyung Miong, Michael Jones and Robert R. Stewart

ABSTRACT

The sensitivity of microseismic source location-estimation on the receiver positions and velocity perturbations are examined via synthetic analyses. The results show that least location error is expected when the receivers are straddling the target formation with a greater aperture (i.e. receiver spacing of 30 m instead of 15 m for an eight-receiver array). Moreover, the effect of velocity perturbation on event location can be minimized when the most optimal receiver configuration is used. The receiver configuration with the smaller aperture tends to increase the sensitivity of the event location on velocity perturbation.

INTRODUCTION

Microseismic monitoring can provide valuable insight into the effectiveness of a stimulation treatment (*i.e.* hydraulic fractures). The ability to dynamically map mono- or multi-stage hydraulic fracture treatments from induced microseisms is a powerful engineering tool to better understand the development and geometry of induced fracture (Le Calvez et. al., 2006). However, interpretational difficulties with microseismic data often arise because of the geometrical configuration of the experiment, and the limited aperture of the receiver array (Drew et. al., 2005). In this paper, various synthetic analysis techniques were used to observe the sensitivity of event location on the receiver configurations and the optimal receiver positions were determined as part of the survey design. Also the sensitivity of event location on a simplified velocity model was explored.

RECEIVER ARRAY DETERMINATION

Velocity model building

Current inversion techniques used for processing microseismic data are based on the determination of time delays between the compressional (P) and shear (S) waves and the polarization angles of the incident P-waves: These parameters provide a distance and azimuth of the microseismic source relative to the receiver, respectively. Hence, P and S-wave velocity models are required to estimate the source locations and to generate a seismogram for synthetic studies. A simplified velocity model is preferred in processing since the velocities from the sonic log tend to fluctuate significantly, which could potentially add complications in locating microseismic events. As shown in Figure 1, a minimum thickness of 3 m was used to block the P-sonic log available from the monitor well where the receivers were deployed: The S-sonic log was blocked using the same interfaces defined for the P-sonic log. The minimum thickness of 3 m for blocking was chosen to simplify the velocity log while capturing the necessary details (e.g. retain the velocity value for the target zone at depth of 1675 m).

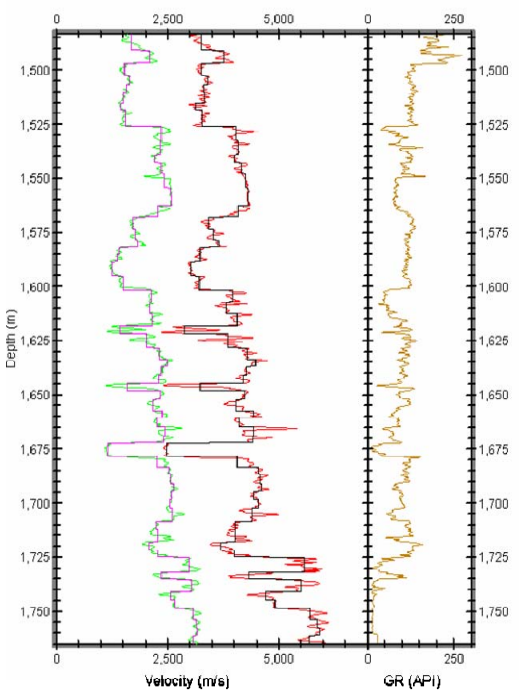

FIG. 1. P (black) and S (pink) velocity models and gamma ray log (light brown).

Synthetic seismogram generation

Assuming that the targeted zone within the treatment well is located at depth of 1675 m and 250 m away from the receivers (red diamond in Figure 2), 20 microseismic events were generated around the target zone with event spacing of 25 m vertically and laterally. The simplified P-velocity (blue curve) and S-velocity (pink curve) models are also plotted on Figure 2 to show the velocity variation within the target zone. The size and orientation of the grid of events are provided in Table 1. Five eight-receiver arrays were virtually deployed in the monitor well; their receiver spacing and top receiver positions are provided in Table 2 and their configurations are shown in Figure 2.

Table 1. Size and orientation of the gridded events.

Number of Events	Event Grid Width (m)	Event Grid Height (m)	Event Grid Azimuth Relative to North
20	75	100	N90E

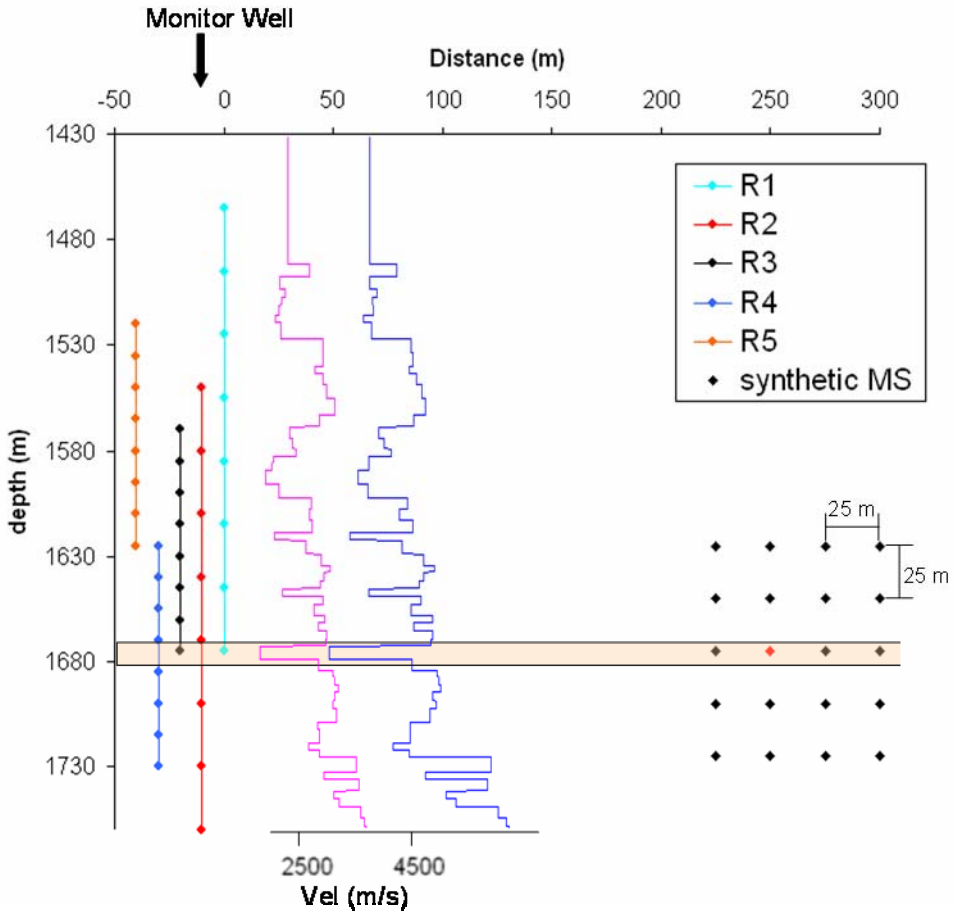

FIG. 2. Positions of receiver arrays and microseismic events. The P (blue curve) and S wave (pink curve) velocities are plotted to reference the target zone.

Table 2. Receiver array configurations used for synthetic analysis.

Receiver Array	Receiver Spacing (m)	Top Receiver Depth (m)
R1	30	1465
R2	30	1550
R3	15	1570
R4	15	1625
R5	15	1520

Given the location of the microseismic events and the velocity of the medium between the source and the receiver, the P and S waves were ray traced through the velocity medium; this response was recorded in each of the eight receivers as a synthetic seismogram. Figure 3 displays a synthetic seismogram for a microseismic source in the target zone (red diamond in Figure 2) recorded by the receiver array positioned above the target zone with 15 m receiver spacing, R3. All events show clear P and S-wave arrivals with high signal-to-noise ratios resulting in stable P and S arrival time picks for the event

location process. This synthetic seismogram was processed using the simplified P and S-wave velocity model (Figure 1) to locate the microseismic source.

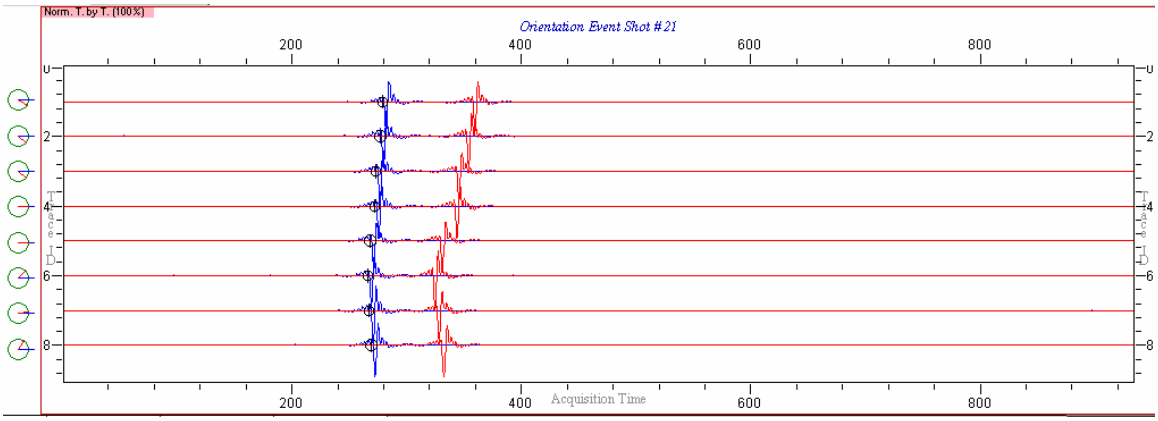

FIG. 3. Synthetic seismogram for a perforation shot (300mE, 0mN, 1625mZ with respect to monitor well) recorded by R3.

Microseismic Data Processing

The estimated locations of microseismic events and their corresponding receiver array are displayed in Figure 4a. The basic concept of the microseismic event-location method is to recreate the travel path of the seismic energy back to its hypocenter. Therefore the objective is to estimate two components; a distance between the source-and-receiver and azimuth of the source relative to the receiver. In a simplified case with the seismic source and the geophone receivers contained in only one medium, a single set of P- and S-waves propagation velocities (V_p and V_s), the range (D) is calculated by measuring the difference in arrival time between P- (T_p) and S-waves (T_s) (ΔT, see Equations1 and 2) (Le Calvez *et.al.*, 2006):

$$\Delta T = T_s - T_p \quad (1)$$

$$D = \Delta T \, (V_p V_s / V_p - V_s) \quad (2)$$

The second component, the directional vector, is determined using hodogram analysis. P-waves oscillate in their direction of propagation; thus, the hodogram indicates a tri-dimensional vector pointing in the direction of propagation. In this simplified case, the resultant vector points straight back toward the hypocenter. With these two parameters (distance, and azimuth) defined, the hypocenter is localized: The complexity of the real-earth model is overcome with more sophisticated ray-tracing algorithms (Figure 4a).

A misfit function is also generated to display an expected accuracy of location-estimation of a single microseismic event (red dot in Figure 4a and contour plots in Figure 4b). The misfit function (Figure 4b) is divided into 560 cells that have a width and height of 25m: Each cell is characterized by varying P- and S-wave velocities. Rays are traced from each corner of these cells to a given receiver position and the arrival time delay between the S- and P-waves is estimated ($\Delta T_{estimated}$). Given the location of the event of interest, the arrival time difference between S- and P-waves is computed

($\Delta T_{observed}$). This value is then subtracted from all the $\Delta T_{estimated}$ values: Hence smaller the misfit contour, more accurate the location estimation is (Equation 3).

$$[\Delta t]_{estimated} - \Delta t_{observed} = [\Delta t]_{misfit} \quad (3)$$

Results and observations

All receiver arrays were able to locate the microseismic events reasonably well and the vertical location estimates exhibited smaller error than the horizontal: This is shown by the elongated shape of the misfit functions computed for all receiver arrays (Figure 4b). For all receiver arrays, the microseismic events in the fifth layer were located at deeper depths than the original depth of the events: The deepest microseismic events occurred in the vicinity of the high velocity layer and the rays emerging from these events were critically refracted (Figure 5). As a result of the refraction, the direct P and S arrival times were delayed.

Considering all twenty estimated event locations, a root-mean-square (RMS) error was computed. The receiver array straddling the target zone with a receiver spacing of 30 m (R2) yielded the smallest RMS location error in both the vertical (± 5.3 m) and horizontal (± 5.7 m) directions (Table 4). The smallest RMS vertical (± 1.7 m) and horizontal (± 5.2 m) errors are also obtained when the events from the fifth layer are omitted for the RMS error analysis.

When RMS errors are computed for each layer of the microseismic events, the vertical and horizontal errors vary inconsistently (Figure 6; right hand side). The receiver array, R3, locates vertical position of the microseismic events at the target zone (i.e. third layer) most accurately; the smallest misfit contour for the event at the target zone (Figure 4b, third misfit function from the top) also suggests that this event is best located by R3 out of all five receiver arrays. However, R3 receiver array locates events poorly in other layers, especially in the second, fourth and fifth layers, compared to R2 receiver array that straddles the target zone.

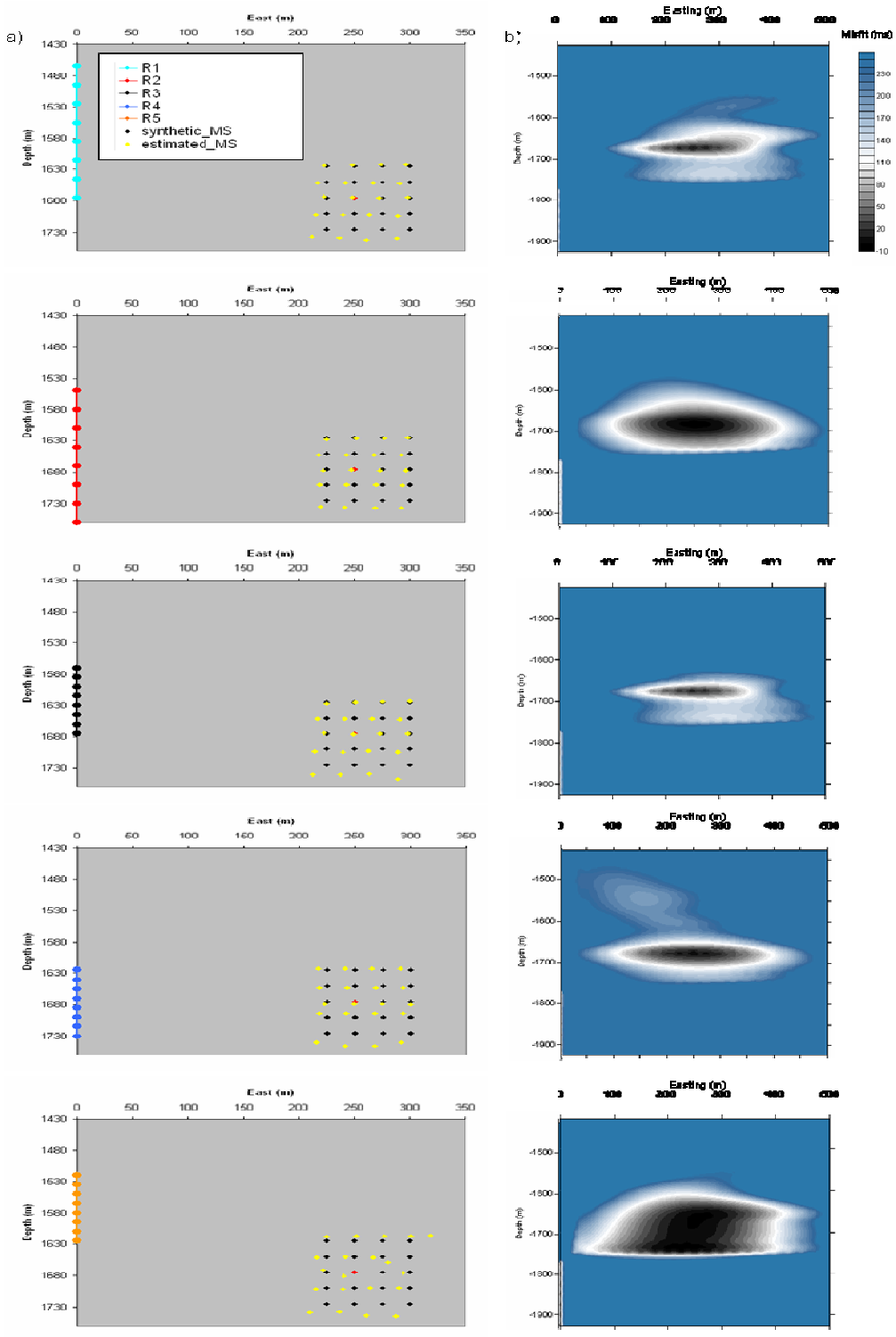

FIG. 4. a) 20 actual (black dots) and 20 estimated (yellow dots) microseismic events with their corresponding receiver array; b) Contours of misfit grid for the event at the perforation (red dots in Figure 2a).

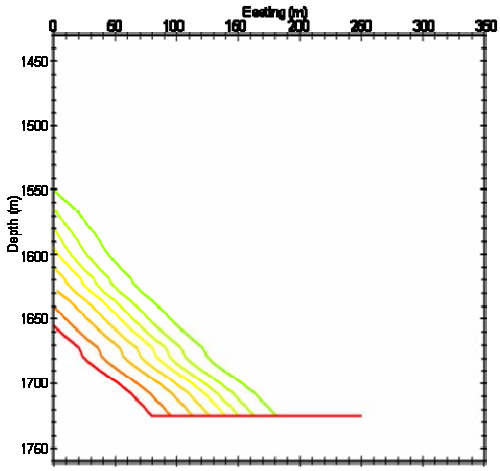

FIG. 5. Critically refract P-rays emerging from an event at fifth row of the microseismic events (250 m E, 0 m N, and 1725 m Z).

Table 3. Root-mean-square errors of event location for four receiver arrays.

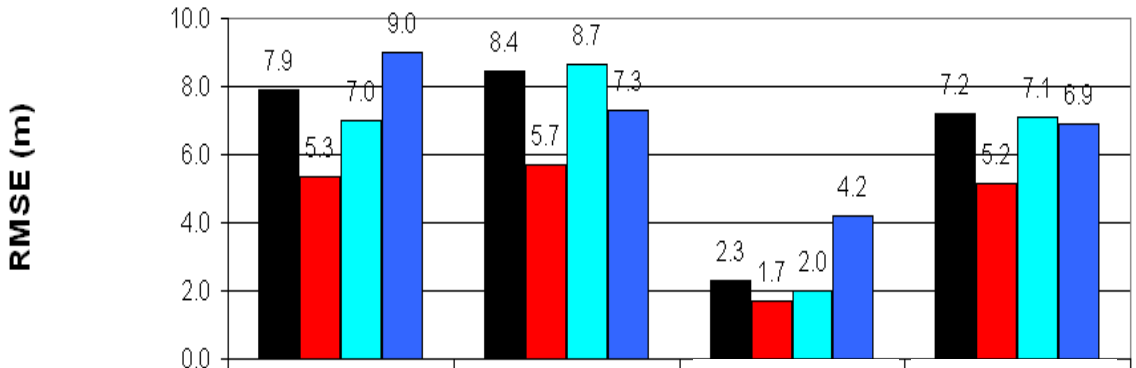

	Z_RMSE for all events	E_RMSE for all events	Z_RMSE for four rows of events	E_RMSE for four rows of events
R3: 15mAbove	7.9	8.4	2.3	7.2
R2: 30mAt	5.3	5.7	1.7	5.2
R1: 30mAbove	7.0	8.7	2.0	7.1
R4: 15mAt	9.0	7.3	4.2	6.9

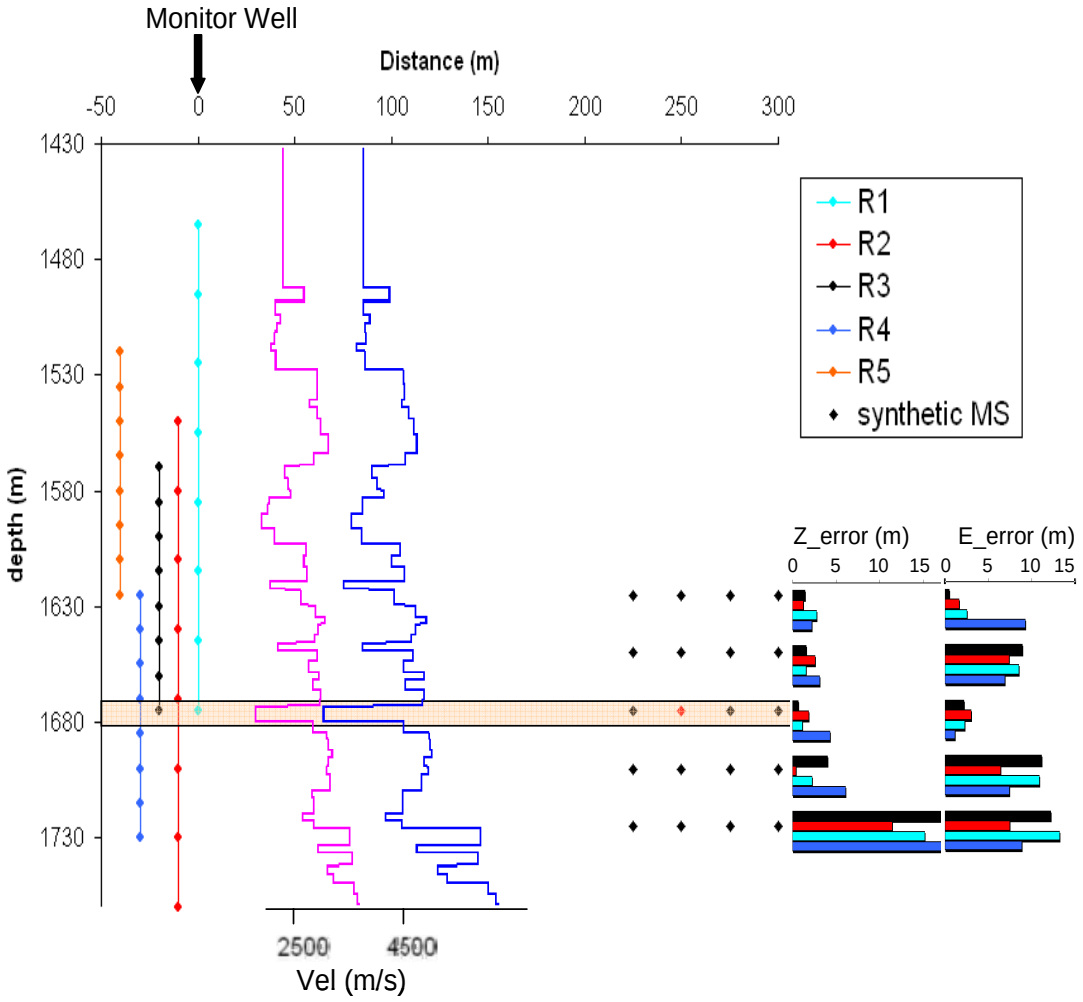

FIG. 6. Positions of five receiver arrays (R1-R5) and microseismic events (black diamond). The P (blue curve) and S wave (pink curve) velocities are plotted to show velocity variation near the target zone; root-mean-square errors of vertical and horizontal estimations for the corresponding to receiver array is plotted for each layer (right hand side, color coded).

EVENT LOCATION SENSITIVITY TEST FOR VELOCITY PERTURBATION AND OBSERVATIONS

The synthetic events recorded by two receiver arrays, one located slightly above the target zone (R3) and the other one straddling the target zone (R2), are processed with the seven set of velocity models with varying level of velocity perturbation. The original 3m-blocked velocity model (Figure 2) was perturbed with a minimum thickness of 4m, 5m, 6m, 7m, 8m, and 9m (Figure 7 and 8). The objective of this exercise was to observe how event location sensitivity changes with the velocity perturbation. As shown in Figure 7, most of the microseismic events in are maintained in the similar locations throughout the velocity perturbation when receivers are positioned at their optimal positions (i.e. R2, receivers straddling the target zone in this case). However, the effect of velocity perturbation is more severe (*i.e.* many events are located in obscure positions) when the receivers are placed at less optimal positions (i.e. R3, Figure 8).

CONCLUSIONS

The synthetic analysis results show that the least location error is expected when the receivers are straddling the target formation with a greater aperture (i.e. receiver spacing of 30 m). The greater aperture improves the geometrical coverage of the receiver relative to the target zone and straddling receivers across the target zone minimizes the time delay when the seismic waves are refracted as they travel through a medium where there is an abrupt velocity increase. Although the events in the target zone can be located with high accuracy with the finer receiver spacing, the smaller aperture tends to increase the sensitivity of the event location on velocity perturbation. The effect of the velocity perturbation on locating microseismic events can be minimized when the most optimal receiver configuration is used. The experiment with the receiver configurations and velocity perturbations reemphasized the importance of using synthetic analysis to explore various geometrical source and receiver configurations prior to the actual survey to optimize microseismic data quality.

ACKNOWLEDGEMENTS

The authors would like to thank CREWES sponsors, especially Schlumberger for providing software for the synthetic analysis in this paper.

REFERENCES

Drew, J., Leslie, D., Armstrong, P., and Michaud, G., 2005, Automated microseismic event detection and location by continuous spatial mapping, Society of Petroleum Engineers, 95513.

Le Calvez, J.H., Tanner, K.V., Glenn, S., Kaufman, P., Sarver, D.S., Bennet, L., Panse, R., Palacio, J.C., 2006, Using induced microseismicity to monitor hydraulic fracture treatment: A tool to improve completion techniques and reservoir management, Society of Petroleum Engineers, 104570.

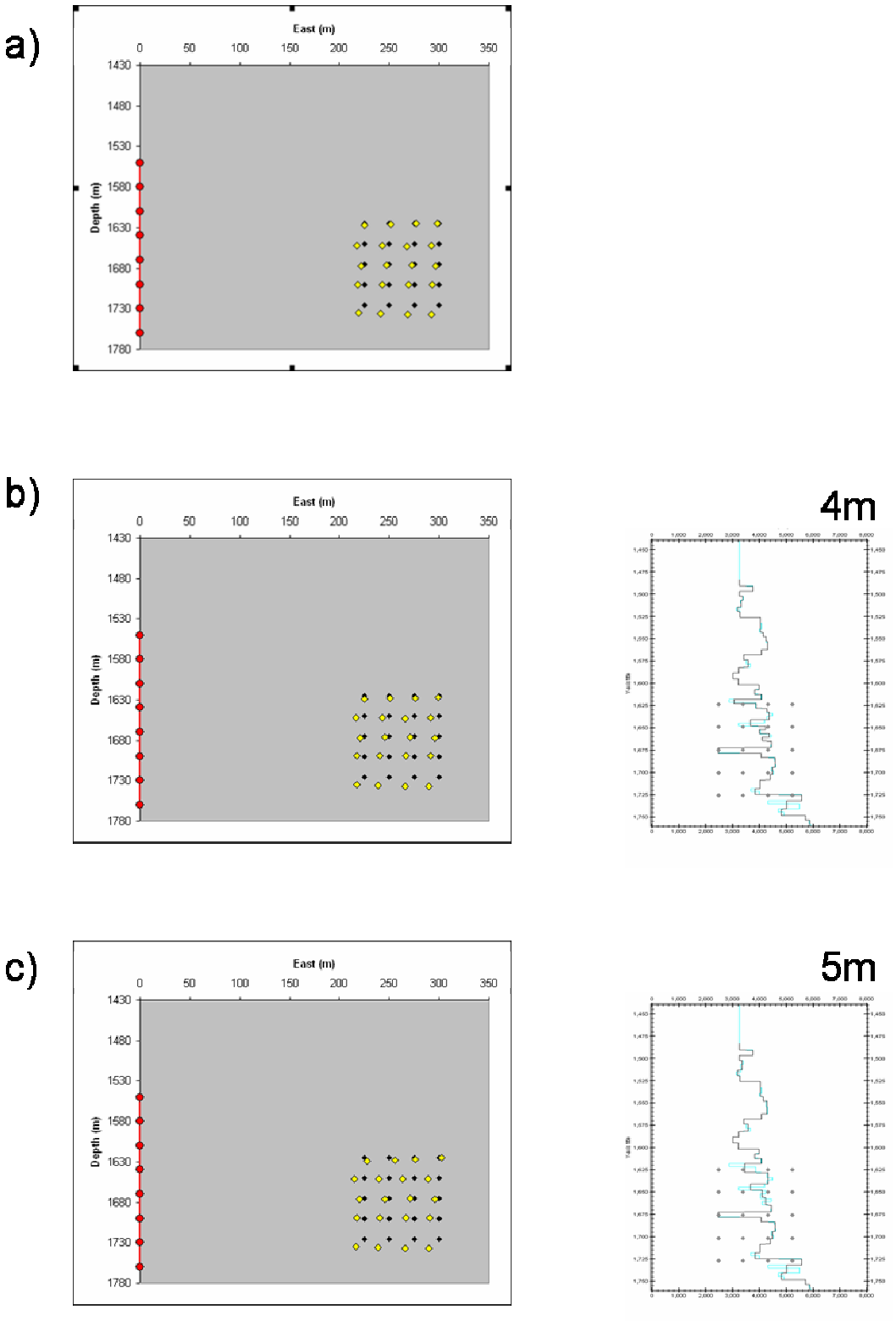

FIG. 7. Event location sensitivity on receiver configuration, R2, and velocity perturbation. The synthetic seismograms are processed with perturbed velocity models where the original velocity model (a) is perturbed with minimum thickness of b) 4m, c) 5m, d) 6m, e) 7m, and f) 8m.

d)

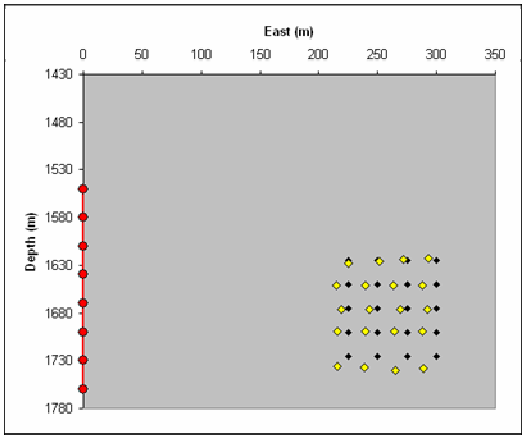
East (m)
0
50
100
150
200
250
300
350
Depth (m)
1430
1480
1530
1580
1630
1680
1730
1780

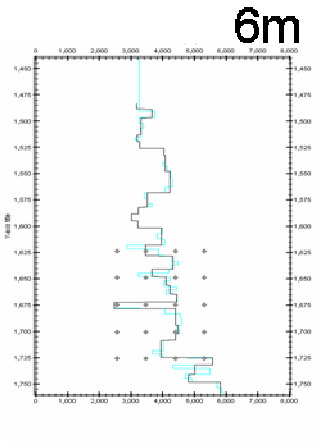
6m

e)

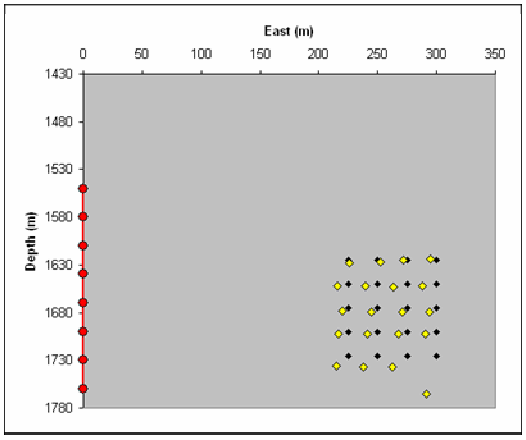
East (m)
0
50
100
150
200
250
300
350
Depth (m)
1430
1480
1530
1580
1630
1680
1730
1780

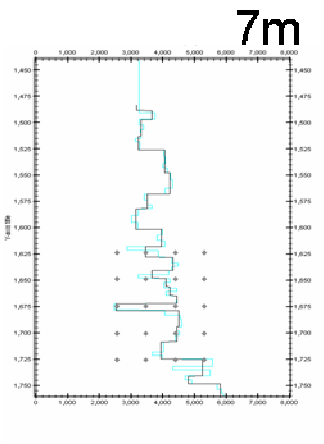
7m

f)

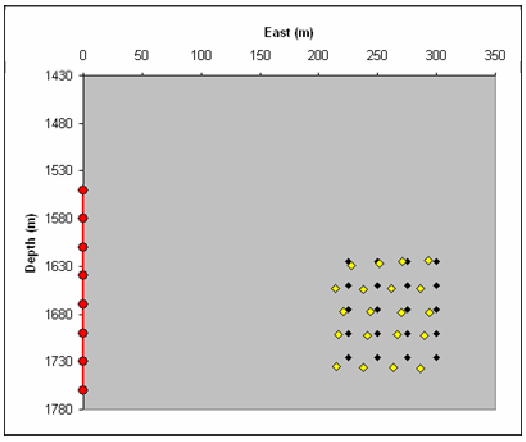
East (m)
0
50
100
150
200
250
300
350
Depth (m)
1430
1480
1530
1580
1630
1680
1730
1780

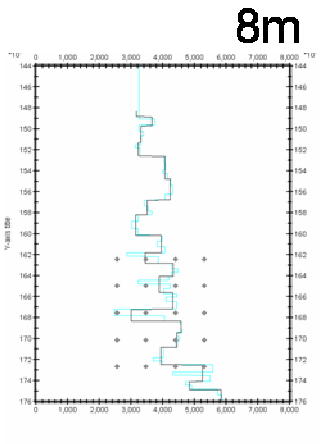
8m

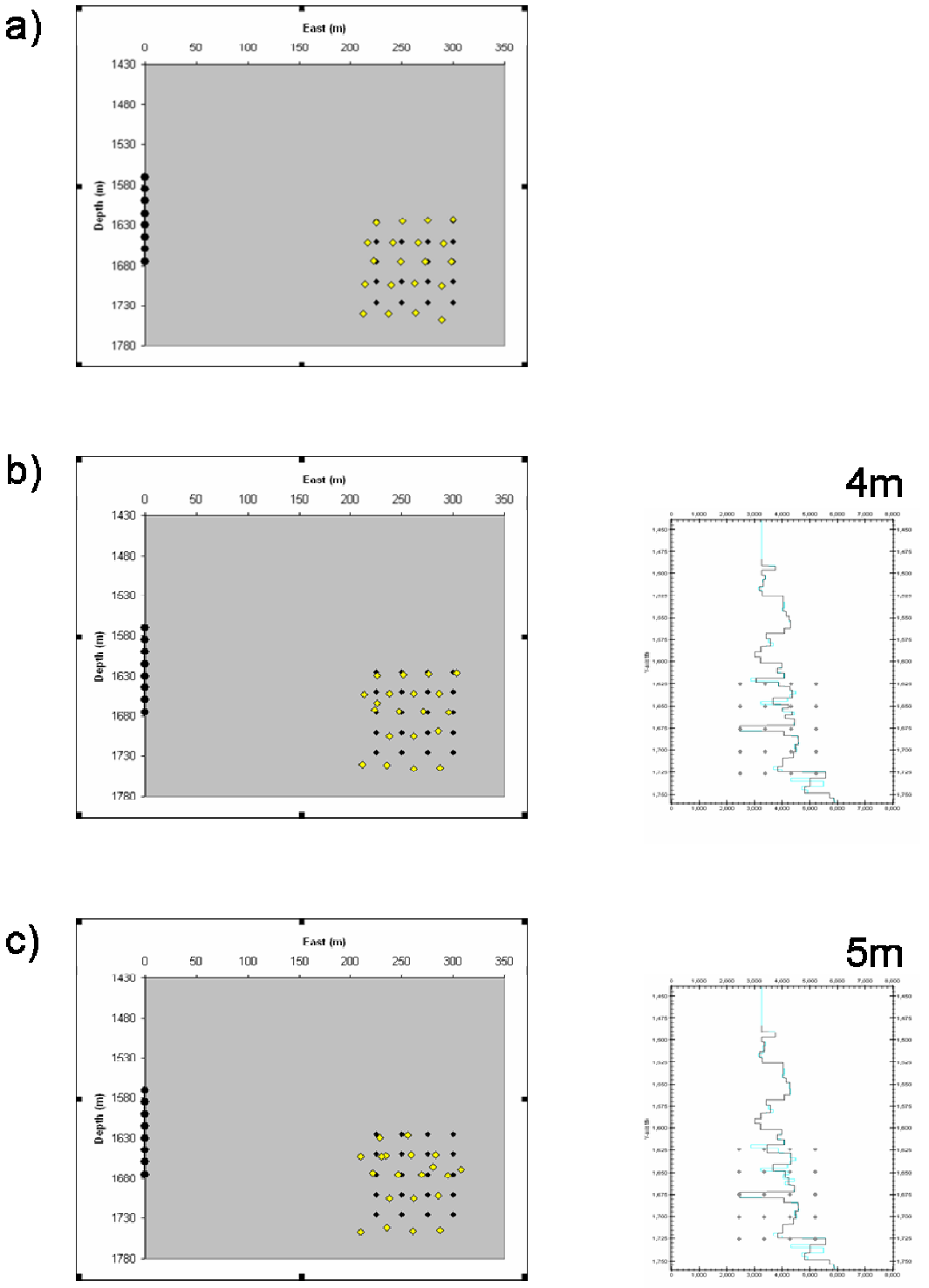

FIG. 8. Event location sensitivity on receiver configuration, R3, and velocity perturbation. The synthetic seismograms are processed with perturbed velocity models where the original velocity model (a) is perturbed with minimum thickness of b) 4m, c) 5m, d) 6m, e) 7m, f) 8m and g) 9m.

d)

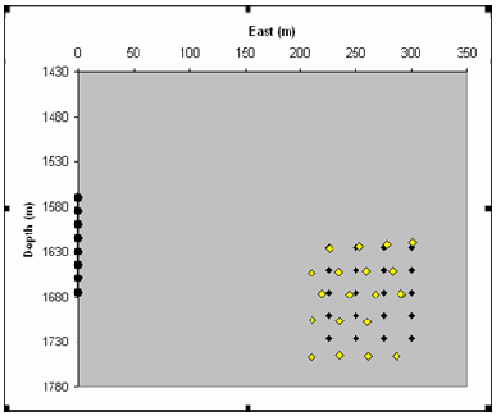

6m

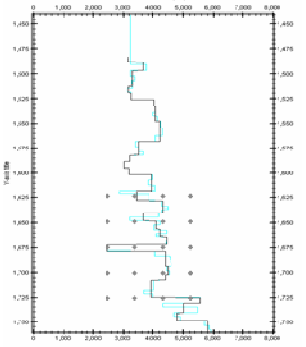

e)

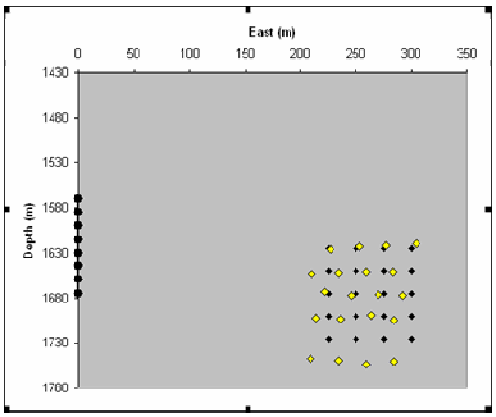

7m

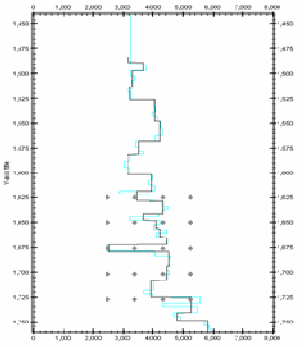

f)

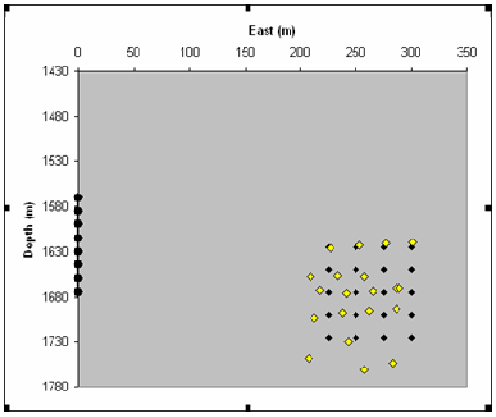

8m

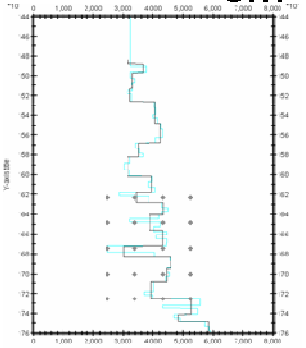

g)

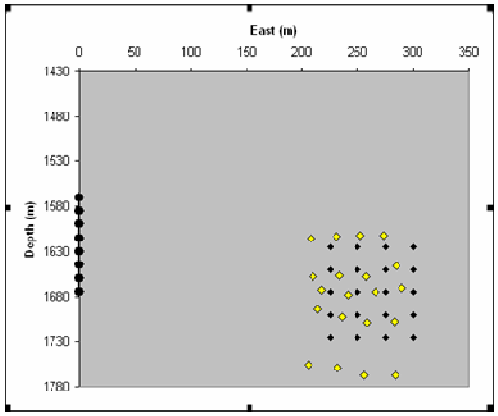

9m